The historic magmatic-hydrothermal eruption of the Breccia di Commenda, Vulcano, Italy

UNIVERSITÀ DEGLI STUDI DI TORINO

THE HISTORIC MAGMATIC-HYDROTHERMAL ERUPTION OF THE BRECCIA DI COMMENDA, VULCANO, ITALY

L Gurioli[1, 2, 3], E Zanella[4, 5], A Gioncada[6], A Sbrana[6],

1 Clermont Université, Université Blaise Pascal, Laboratoire Magmas et Volcans, BP 10448, F- 63000 Clermont Ferrand, France
2 CNRS, UMR 6524, LMV, F-63038 Clermont-Ferrand, France
3 IRD, R 163, LMV, F-63038 Clermont-Ferrand, France
4 Dipartimento di Scienze della Terra, Università di Torino, Torino, Italy
5 Alpine Laboratory of Paleomagnetism (ALP), Peveragno, Italy
6 Dipartimento di Scienze della Terra, Università di Pisa, Pisa, Italy

Corresponding author: Lucia Gurioli
Laboratoire Magmas et Volcans, Univ. Blaise Pascal-CNRS OPGC,
5 rue Kessler 63038 Clermont Ferrand FRANCE
Tel: +33 (0)473346782
Fax: +33 (0)473346744
L.Gurioli@opgc.univ-bpclermont.fr

Abstract

The historic Breccia di Commenda (BC) explosive eruption of Vulcano (Aeolian Islands, Italy) opened with a phase that generated a grey fine ash layer dispersed to the northwest (Phase 1). The eruption continued with a dilute pyroclastic density current (PDC) that was dispersed to the east, followed by the emplacement of radially distributed, topographically controlled PDC deposits (Phase 2). The last phase of the eruption produced a sequence of accretionary lapilli and grey fine ash dispersed toward the southeast (Phase 3). The most impressive feature of the BC is its high lithic/juvenile clast ratio and the yellow color of the deposits of Phase 2. Lithic fragments are mainly hydrothermally altered rocks, in the silicic and advanced argillic facies. Juvenile fragments, ranging from 20% to 40% by volume, are mainly confined to the ash component of the deposits and comprise rhyolitic to trachyandesite, poorly to non-vesicular fragments. The fine ash fraction of the deposits is richer in S, Cu, Zn, Pb, and As than the BC juvenile lapilli and bombs, and also the juvenile

components of other La Fossa units, suggesting that the BC formed in the presence of an anomalously high amount of S and metals. Sulfur and metals may have been carried as aerosols by chloride- and sulfate-bearing micro-crystals, derived from the condensation of magmatic gas in the eruptive cloud. The high content of hydrothermally altered lithic clasts in the deposits suggests that explosions involved the fluid-saturated hydrothermally altered rocks residing in the conduit zone. However, the presence of a juvenile component in the deposits supports the idea that this explosion may have been triggered by the ascent of new magma. We categorize this eruption as magmatic-hydrothermal, to emphasize that in this type of phreatomagmatic eruption the external water was an active hydrothermal system.

Rock magnetic temperatures of non-altered lava lithic fragments indicate a uniform deposit temperature for the PDC deposits of between 200 and 260 °C, with a maximum at 280 °C. These homogeneous, relatively low temperatures are consistent with the idea that the Phase 2 explosions involved the expansion of abundant steam from the flashing of the hydrothermal system. In addition, recent paleomagnetic dating of the BC provides an age of between 1000 and 1200 AD, younger than that reported in the previously published data, suggesting that previous interpretations and the recent history of La Fossa and Mt. Pilato require re-evaluation.

Key words: Phreatomagmatic, magmatic-hydrothermal eruptions, eruptive mechanisms, hydrothermal systems, Vulcano.

Introduction

At volcanoes characterized by intense hydrothermal activity, eruptions may produce deposits extremely rich in hydrothermally altered lithic (that is, non-juvenile) clasts and subordinate juvenile fragments (e.g. Browne and Lawless 2001). According to these authors, “if the explosion derives solely from heat loss and phase changes in a convecting hot water- or steam- dominated hydrothermal system, it is defined as a hydrothermal eruption” (Browne and Lawless 2001, page 300). “If injection of magma into a pre-existing hydrothermal system causes a heat pulse that triggers the eruption”, it can be termed a magmatic-hydrothermal eruption. In the latter case, “the bulk of the energy responsible for the eruption is derived from the hydrothermal system itself, but the magmatic input has an essential triggering role” (Browne and Lawless 2001, page 300). Examples of magmatic-hydrothermal eruptions include the eruption that produced the yellow deposits at Galeras (Calvache and Williams

1992), the 550 BP eruption at Inyo Crater (Mastin 1991), and the 1967-1977 eruptions at La Soufrière de Guadaloupe (Sheridan 1980; Wohletz and Heiken 1992). As pointed out by Browne and Lawless (2001, page 300), "this terminology has not been formally defined in the literature", because these eruptions are a subset of the phreatomagmatic category. We use it here, however, to emphasize the strong involvement of an active hydrothermal system in the eruption. We propose that another example of such activity is represented by the Breccia di Commenda (BC hereafter), which was produced by an historical explosive eruption that occurred at La Fossa volcano, Vulcano, Aeolian Islands, Italy around the sixth century according to Keller (1970, 1980). The BC eruption has been previously considered as purely phreatic (Frazzetta et al. 1983), but juvenile components have been recently recognized in the deposits, indicating that magma was involved in the event (Gioncada et al. 1995; Dellino and La Volpe 1997; Gurioli and Sbrana 1999).

La Fossa is an active volcano, the last eruption of which occurred in 1888-90 (e.g. Keller 1980). A hydrothermal system, linked to magma at a depth ≤4 km (Clocchiatti et al. 1994; Gioncada et al. 1998), has been active at La Fossa at least since the BC eruption (Fulignati et al. 1998; Boyce et al. 2007). Several deposits related to post-BC explosive events are also characterized by a large amount (more than 50% by volume) of hydrothermally altered lithic fragments (e.g. Keller 1980; Frazzetta et al. 1983). However, the BC is the largest and the most widely dispersed within these hydrothermally altered lithic-rich deposits (Dellino 1997), indicating that the BC eruption is relevant to volcanic hazard evaluation at Vulcano (Gurioli and Sbrana 1999; Dellino et al. 2011).

In this paper, we describe the BC with the objective of establishing emplacement dynamics. Then we present petrographic and geochemical data for the different components of the deposit to give information on the juvenile and lithic components involved in the explosive process. Next, rock magnetic measurements on the lithic fragments are used to quantify the temperature of emplacement and provide an estimate of the age of the eruption. Finally, all data are used to reconstruct the eruption mechanisms, to propose a possible eruptive scenario, and to make inferences regarding the volcanic hazard presented by this type of eruption at Vulcano.

Geological framework

Vulcano is a volcanic complex belonging to the Quaternary Aeolian island arc (Barberi et al. 1994). Together with Lipari and Salina, Vulcano (Fig. 1a) forms a roughly N-S trending

volcanic chain, located inside a deep graben (Barberi et al. 1994). This structure is linked to a regional strike-slip structure, the Aeolians-Tindari-Letoianni lithospheric discontinuity (Barberi et al. 1994). Vulcano's products are all post-marine oxygen isotope stage (MIS) 5e (Lucchi et al. 2004). La Fossa volcano is the current active center of the island and is a small composite tuff cone, slightly elliptical in shape, with a diameter of about 1 km and a maximum elevation of 300 m a.s.l. (Fig. 1a). The cone has grown over the last 6000 years (Frazzetta et al. 1983) within a collapse structure with an area of about 7 km^2 (Fig. 1a). This collapse structure is related to the development of a pull-apart basin (Barberi et al. 1994; Ventura 1994) and derives from the coalescence of several collapses that have occurred since 50 ka (De Astis et al. 1989; Gioncada and Sbrana 1991). La Fossa's volcanic stratigraphy has been described by Keller (1980), Frazzetta et al. (1983, 1984), Frazzetta and La Volpe (1991), Dellino and La Volpe (1997) as well as Gioncada et al. (1997). De Astis et al. (2006) produced a new geological map of the island (Fig. 1b). Eight different formations have been distinguished in the deposits of La Fossa (Fig. 1b), on the basis of the main unconformities present. The Punte Nere Formation comprises the majority of the cone (Fig. 1) and consists of shoshonitic to trachytic phreatomagmatic pyroclastic density current (PDC) and fall deposits, and ends with trachytic lava, dated at 3800 +/- 900/800 years ago using Uranium-series disequilibria (Soligo et al. 2000).

The Caruggi Formation (Fig. 1b) contains the BC (ca1, De Astis et al. 2006) and mainly consists of PDC and minor fall deposits (Fig. 1b). Thick deposits of very thinly bedded, varicolored tuffs (ca2, De Astis et al. 2006) lie above the BC. The BC eruption was contemporaneous with the Mt. Pilato activity of Lipari (Fig. 1), as indicated by laminae of rhyolitic ash correlated with the Upper Pilato Pumice (UPP; Keller 1980; Frazzetta et al. 1983) interbedded with the BC (Fig. 2). Following Keller (1970, 1980), the BC event has always been assigned to the sixth century, because the UPP occurs on Roman ruins of the fourth and fifth centuries AD at Contrada Diana, near Lipari, on Lipari Island (Keller 1970). Fission track dates on the ash confirmed that it and the BC were erupted in the sixth century (Bigazzi and Bonadonna 1973). Recent paleomagnetic work has revised the age of volcanic activity for both La Fossa and Vulcanello (Arrighi et al. 2006; Zanella 2006), suggesting a new, younger age (1000-1200 AD) for the BC.

Since Vulcano's last eruption in 1888-1890, La Fossa has been characterized by fumarolic activity of variable intensity and temperature (up to 690 °C, Chiodini et al. 1995). Mineralogical and geochemical studies of the surficial and subsurface altered rocks indicate the presence of an active high-sulfidation-type hydrothermal system (Fulignati et al. 1998,

1999; Boyce et al. 2007) linked to the ascent of acidic gases (SO_2, HCl, HF) released from a shallow magma (Clocchiatti et al. 1994; Gioncada et al. 1998).

Methods

Field-based analyses

Field-based analyses included mapping, logging, and sampling of several outcrops around La Fossa (Figs. 1a, 2 and 3, Supporting Material 1). The nomenclature used in the classification of bed thickness, grain size, sorting, and the criteria used in interpretation follow those of Sohn and Chough (1989) and Chough and Sohn (1990). Grain size and component analyses were completed on 45 samples from different sites and stratigraphic positions (Supporting Material 1), following the procedure proposed by Barberi et al. (1989). Because of the pervasive alteration of the clasts, however, we obtained the componentry data by point counting of the 1 ϕ grain size class in thin section, which corresponds to the main mode in all samples (Figs. 4 and 5). Tests on a few samples showed that the finer grain size classes (2 ϕ and 3 ϕ) have a very similar distribution of components (Gurioli 1994). Therefore, the 1 ϕ class can be considered representative of the coarse ash of the deposits. We counted at least 750 points per thin section and based on the Van Plas and Tobi (1965) chart, we made an error up to 3.5%. The error could be greater for the coarse-grained deposits in which the coarse ash comprises less than 50 volume % (section 3, Fig. 5a).

Compositions

X-ray fluorescence (XRF) analyses of major and trace elements were performed on the juvenile lapilli and bombs and on the fine ash of the BC at the Dipartimento di Scienze della Terra (University of Pisa) using a Philips PW 1480 spectrometer. Correction for matrix effects was carried out following Franzini et al. (1975). Accuracy was monitored using international standards and was 10% for the trace elements having concentrations around 10 ppm and less than 10% for higher concentrations. Loss On Ignition (LOI) was determined at 950 °C on powders dried at 105 °C. Magnesium and sodium were obtained by atomic absorption spectrometry and ferrous iron by titration. Microanalyses of the glass and mineral phases were carried out with a Philips XL30 scanning electron microscope equipped with microanalysis EDAX (standardless software DXi4), 20 kV acceleration voltage, 5 nA beam current and 100 s live time. The accuracy is better than 0.5% if the abundance is >15 wt.%, 1% if the abundance is around 5 wt.%, and better than 20% if the abundance is around 0.5 wt.%.

Paleomagnetism

Lithic clasts (2 to 10 cm in diameter), mostly unaltered trachyte lavas from the previous eruptions, embedded in the PDC deposits were sampled at ten sites around La Fossa cone (Fig. 1a). Section 5 (Figs. 1a and 2b) was further sampled at five different stratigraphic heights (from layer *2a* up to the top of layer *2c*, Figs. 2a and 2b). At four sites, clasts larger than 5 cm in diameter were oriented using both magnetic and solar compass and clinometer. In this case, magnetic analyses provided the temperature of the deposit as well as the absolute paleomagnetic direction. At other sites, the small clast size prevented accurate orientation, and these little clasts were used only for deposition temperature. For each site, at least ten clasts were collected and cut in the laboratory to obtain two or more specimens from each clast.

The temperature of the deposit ($T_{dep,}$ Cioni et al. 2004) was estimated according to the procedure of Cioni et al. (2004) and Zanella et al. (2007, 2008). Measurements were carried out at the University of Torino's Alpine Laboratory of Paleomagnetism (Peveragno–Italy) using a JR-6 spinner magnetometer and Schonstedt furnace. Progressive thermal demagnetization was carried out on 136 specimens. To improve accuracy in the T_{dep} estimate, two runs shifted by 20° C were completed for each site, one starting at 60 °C, the other at 80 °C. Each run consisted of heating in steps of 40 °C up to maximum temperatures of 540-560 °C, which were sufficient to erase all the natural remanent magnetization (NRM). Magnetic susceptibility was measured after each step to check for alteration caused by heating and no significant change was observed. Zijderveld (1967) diagrams and Principal Component Analysis (PCA) (Kirschvink 1980) were used to isolate the low- and high-temperature remanence components of single clasts, and compute their directions in cases where they had been oriented. T_{dep} at each site was then obtained from the overlapping reheating ranges for all lithic clasts collected at that site (Cioni et al. 2004).

The pre-eruptive environment

The BC lies on an erosion surface cutting lava and pyroclastic facies. This surface is coated by a mm- to cm-thick crust that is best developed in the eastern sector of the volcano. The crust resembles brown-red enamel paint and is composed of glass shards and crystals cemented by silica and minor sulfate minerals. This crust is very similar to the crusts that currently occur widely on surfaces across La Fossa cone. These crusts are thought to result from exposure of the ground surface to the acidic plumes produced by La Fossa's active fumaroles (Fulignati et

al. 2002). A similar case-hardened crust on erosion surfaces at Kilauea has been attributed to an acidic environment (Malin et al. 1983; Naughton et al. 1976).

The BC

The BC consists of several mappable layers produced by three successive eruption phases of characteristic style (Figs. 1b and 2).

Phase 1

The lowermost layer consists of grey, massive, fine to coarse ash (Figs. 2b and 2c). The thickness is constant over the scale of an outcrop, and up to 10 cm in the most proximal outcrops (Fig. 2f, Supporting Material 1). The dispersal is poorly constrained due to the paucity of outcrops west of La Fossa cone, but broadly northwesterly (Fig. 3a). The deposit covers an area greater than 5 km^2. In the western sector of La Fossa, it is interbedded with white rhyolitic ash (Fig. 2f) of the UPP (Keller 1980; Frazzetta et al. 1973). The UPP (Fig. 2) is very easy to recognize and provides a prominent marker horizon on La Fossa (e.g. Frazzetta et al. 1983). The UPP is composed of aphyric glass shards and minor pumice fragments, that are much more evolved in composition than the products of La Fossa (Table 1).

On La Fossa's eastern slopes, the Phase 1 deposit is grey-purple, contains accretionary lapilli, and overlies the white UPP (Fig. 2c). Its upper and lower boundaries are sharp and planar. There is no soil, hydrothermal crust or any other features that would suggest a time break between this deposit and the UPP or Phase 2 deposits. Locally, UPP and Phase 1 ash have been eroded by the PDC related to Phase 2 deposits (Supporting Material 1).

Phase 2

The deposits of Phase 2 consist of four main layers (named *2a* through *2d*, Figs 2, 4 and 5). The contacts between the layers are generally gradational, but locally sharp and erosive. Layers *2a*, *2b*, and *2d* have been described only in the eastern sector up to the distal locations of the Caruggi area (Figs. 1 and 3b). In contrast, layer *2c*, which is the thickest, is dispersed all around La Fossa (Fig. 3b). These deposits show a distinctive yellow color that contrasts with the grey color of the underlying (Phase 1) and overlying (Phase 3) pyroclastic deposits.

Layer 2a

Layer *2a* lies directly on Phase 1 grey ash or on the UPP (Figs. 2c and 5). It consists of yellow, poorly sorted, stratified to massive, lithic-rich, lapilli and coarse ash deposits up to 100 cm thick (Fig. 2). Thickness and facies variations are topographically controlled. In the southern sector at the base of La Fossa where the paleosurface was relatively flat, layer *2a* consists essentially of one yellowish bed (up to 10 cm thick) of lapilli and coarse ash, and appears more continuous than on La Fossa slopes (Figs. 2b and 2c; Fig. 5a, section 5). In paleo-gullies on the flanks of the cone, layer *2a* is lenticular (0 to 100 cm thick, sections 45 and 30a, Fig. 5b). Where the deposits thicken and coarsen into topographic lows, layer *2a* is well stratified (Fig. 5b, section 30b) and comprises alternating, reversely graded coarse ash and lapilli layers, both of which are fines-poor (Fig. 5b). Where layer *2a* rests on the UPP, the contact is sharp. Layer *2a* samples have a sorting value between 1.5 and 2.5 (Fig. 4). The grain size distribution is bimodal: a main mode occurs at 0-1.5 ϕ and a subordinate (coarser) mode occurs between -1 and -3 ϕ (Fig. 5). Where the deposit is stratified, single layers are well sorted and have a unimodal distribution (Fig. 5b, section 30b). In the southeastern and eastern sectors of La Fossa, layer *2a* is rich of blocks and bombs chaotically mixed with fragments of the substratum, such as UPP or alteration crusts (Fig. 2e, and Fig. 5c, section 49). The grain size distribution at these locations includes a coarse mode at about -4 ϕ and a finer mode at about 1 ϕ (Fig. 5c, section 49).

Layer 2b

Layer *2a* is overlain by a 15-cm-thick, normally graded layer that consists of yellowish, well-sorted, fines-poor, lithic-rich, coarse ash and lapilli (layer 2*b*, Figs. 2c and 5). The bed has crude parallel laminae (Fig 5c, section 49) or low-angle cross-laminae (Fig 5a, section 5 and Fig 5b, section 45). The parallel laminae are visible at the foot of La Fossa and in the Caruggi area (Fig. 1), whereas the cross-laminae occur on the steep flanks of La Fossa. The laminae are commonly defined by normally graded, fines-poor lapilli alternating with well sorted coarse ash laminae. The contact with the overlying layer *2c* is generally gradational. The contact with layer *2a* is planar and enhanced by the grain size difference between these two layers. In section 49 (Fig 5c), vertical pipe-like, gas-escape structures several centimeters long, start above lithic blocks of layer *2a*, cut the laminae in layer *2b* and terminate at the base of the overlying layer *2c*. Therefore, these gas-escape structures formed probably by immediate post-depositional steaming of the larger hydrothermally altered lithic clasts of layer *2a*. Layer *2b* samples have a single mode around 1 to 2 ϕ (Figs. 4 and 5). There is no significant variation in grain size with distance from the vent (Fig. 5).

Layer 2c

Layer *2c* comprises yellow, massive to reversely coarse-tail graded, poorly sorted, lithic-rich ash, lapilli and blocks (Fig. 2). On the southern, southeastern and eastern slopes of La Fossa, these deposits extend continuously from elevations of about 200 m to the base of the cone on slopes of less than 18°. The maximum outcrop elevation occurs on the relatively flat top of the Commenda lava on the southwestern flank of La Fossa (Fig. 3b). Several outcrops beyond La Fossa cone occur in the southeastern sector and more rarely in the northern sector (Fig. 3b). Layer *2c* covers an area of at least 11 km^2, and has a volume of about 0.002 km^3 (Gurioli and Sbrana 1999). Layer *2c* is mainly composed of blocks and lapilli clasts embedded in a yellowish, fines-poor, coarse ash matrix (Fig. 4). The deposits in the western sector are distinctly red (Fig. 2f). Layer *2c* is thicker (up to 4 m) and coarser in topographic lows whereas it is thinner (5 cm) and finer on topographic highs (Figs. 4 and 5). The bomb and block content is about 20% in volume, although lower and higher concentrations occur locally, and the layer is finer grained with distance from the vent. Multiple beds, mainly defined by reverse grading of clasts coarser than 8-10 cm, are generally present (Fig 5a, section 5), although multiple normally graded beds occur locally where the deposits are thicker at the base of La Fossa (Fig. 5a, section 3). Elongate blocks are imbricated. At the base of the layer is a thin (1-10 cm in thickness), coarse ash and lapilli bed which is faintly laminated in its upper part (Fig 5a, section 3). In the topographic low of the Palizzi area where the maximum deposit thickness is observed, several degassing pipes occur in the upper portion of the deposit (Fig. 5a, section 3). The deposits of layer *2c* (Fig. 5) have a bi- to poly-modal grain size distribution; the fine mode is about 1 to -1 ϕ, and the coarse mode is about -4 and -2 ϕ. In the thin deposits on topographic highs (Fig 5b, section 30a) or in more distal sections, the grain size distribution is negatively skewed. In the thickest and coarsest deposits, where blocks represent 50% of the volume, the coarser mode is at -8 ϕ (Fig. 5a, section 3).

Layer 2d

Layer *2d* consists of lenses (5-10 cm thick) of brown-yellow, massive, well-sorted coarse ash above an erosion surface cutting layer *2c* in section 48 (Figs. 2d, 4). Layer *2d* is covered by the UPP ash.

Phase 3

Phase 3 is represented by at least three massive layers with a total thickness of 30 cm (Supporting Material 1). They are composed of alternating accretionary lapilli-bearing indurated grey ash and coarse ash (Figs. 2a and 2d). The deposits are poorly sorted and coarse grained due to the presence of lapilli up to 10 mm in diameter (Fig. 4). Laminae of UPP ash

are commonly interbedded with these deposits. These deposits have been observed dominantly in the southern and eastern sectors of La Fossa, suggesting dispersal toward the southeast, and cover an area greater than 6 km^2 (Fig. 3c). The maximum thickness is reached on the southeastern side of La Fossa and the degree of induration diminishes with distance from the cone.

Component analysis

The relative abundances of juvenile clasts, loose crystals (clinopyroxene, plagioclase, K-feldspar, and rare olivine) and lithic clasts in the BC were assessed.

Juvenile clasts

Poorly vesicular (<30 volume % vesicles) to dense coarse ash, lapilli and bombs characterized by fresh, microlite-poor, glass were interpreted as juvenile fragments (Fig. 6a). A few of the juvenile clasts are moderately vesicular (~ 40 volume %) and have elongate vesicles. Many juvenile lapilli and bombs have fine ash adhering to surfaces and filling vesicles, however, they are distinguished from non-juvenile clasts by the lack of pervasive alteration. The adhering ash consists of fresh glass shards and lithic fragments and crystals (clinopyroxene, feldspar, alunite) and amorphous silica. The glass shards have a patinae formed by alterd rims 3-5 microns thick, composed of smectite-like phyllosilicates. However, we considerd the glass shards to be juvenile because they lack of pervasive alteration.

The composition of the juvenile clasts varies in the different phases of the eruption. Phase 1 deposits contain trachytic to rhyolitic juvenile clasts. Phase 2 deposits have the largest compositional range (SiO_2 62 to 75 wt.%, Table 1). The Phase 3 deposits are largely rhyolitic in composition.

The phenocryst assemblage within the juvenile clasts consists of sanidine, K-feldspar-mantled plagioclase, Ti-magnetite and biotite in rhyolitic and trachytic clasts, whereas plagioclase and clinopyroxene prevail in trachyandesitic clasts. Biotite has been replaced by a mass of <10 micron opaque minerals. In general, the phenocrysts (between 0.2 and 3 mm) are euhedral and range from 5 to 20% in volume, but the average is around 5 to 8% in volume (Gurioli 1994). The crystallinity of the groundmass is mostly low (up to 3% in volume), and groundmass glass compositions range from trachyandesite to rhyolite (Fig. 6b, Table 1).

Textures suggestive of mingling of trachyandesite-trachyte in a rhyolitic host, common in La Fossa products, have been observed. Some rhyolitic clasts contain enclaves of plagioclase and clinopyroxene phenocrysts in a holocrystalline groundmass.

Lithic clasts and crystals

Lithic fragments are the most abundant constituent of the deposits. Four classes are present (described in order of decreasing abundance):

(i) Hydrothermally altered lava and tuff clasts. These clasts are intensely altered to combinations of silica, alunite and minor Ti-oxide phases and cut by late jarosite veinlets. Intense alteration has obliterated the primary lithology. The alteration mineralogy and its pervasive nature correspond to the silicic (mainly composed of residual silica) and advanced argillic (mainly composed of alunite) facies, typical of the upper part of high-sulfidation hydrothermal systems and already described at the present La Fossa crater (Fulignati et al. 1998; Boyce et al. 2007). These characteristics suggest that the provenance of these altered clasts is the upper part of the volcanic conduit.

(ii) Unaltered trachytic lava clasts. These clasts have phenocrysts of plagioclase, sanidine, augite and minor olivine in a holocrystalline trachytic groundmass made of the same minerals; abundant feldspar laths in the groundmass show a preferred orientation. Their characteristics match La Fossa trachytic lavas exposed on the cone (Gioncada 1997).

(iii) Altered flow-banded rhyolite clasts, characterized by the presence of Fe-hedenbergitic clinopyroxene in a quartz-feldspar groundmass. Lithophysae with quartz, tridymite and hematite crystallised in vugs are common. These clasts are interpreted as fragments of rhyolitic plugs occupying the conduits of older eruptions (Clocchiatti et al. 1994).

(iv) Slightly altered dolerite clasts. These clasts have plagioclase and clinopyroxene phenocrysts in a medium-to-coarse grained intersertal groundmass of the same minerals. Because they do not resemble any exposed lavas and the groundmass is coarse grained, we infer they come from subvolcanic intrusions.

Rare phlogopite- and talc- altered lavas and subvolcanic rocks, corresponding to high-temperature magmatic-hydrothermal alteration facies (Fulignati et al. 1998), were observed. Salitic to Fe-hedenbergitic clinopyroxene and garnet-bearing rocks probably result from contact metamorphism and metasomatism involving magmatic brines (Boyce et al. 2007).

The crystal population is mainly composed of plagioclase and pyroxene and subordinate K-feldspar (up to 2% in volume) and rare olivine. Because of the pervasive alteration of the plagioclase and pyroxene, we consider the crystals non-juvenile, although the 2% in volume of K-feldspar is probably juvenile, because of its fresh appearance.

Components abundance in the BC deposits

Relatively low juvenile clast abundance is the main macroscopic characteristic of the deposits (Fig. 7, Supporting Material 1). Indeed, in the coarse ash, the juvenile fraction ranges from 20% up to 40% in volume, the crystal content varies from 10 to 30% and the lithic content ranges from 40 to 70% in volume (Supporting Material 1).

In the deposits of Phase 1, the lithic component represents about 60 volume % of the coarse ash and it has the highest content of trachytic lavas (34 volume %, Fig. 7).

In the deposits of Phase 2, the coarse ash shows a higher abundance of juvenile components with respect to Phase 1. The bottom of layer *2a* has the highest juvenile content of all layers (40 volume %, Fig. 7 and Supporting Material 1). In the eastern distal section (in the Caruggi area), layers *2a* and *2b* have slightly higher lithic component abundance, due mainly to an increase in the abundance of hydrothermally altered fragments (Fig. 8). Layer *2c* has similar componentry from the base to the top (Fig. 7), but the lithic clast abundance is higher in the ash-rich facies (although the relative proportions of the different lithic fragments types are the same) and in the deposits in the western sector (Fig. 8).

Phase 3 deposits (Fig. 7) are characterized by the highest content of crystals (30 volume %, Fig. 7). The lithic clast population shows the highest content of flow-banded rhyolite fragments (20 volume %) and a lower content of hydrothermally altered rocks (45 volume %).

Fine ash (<63 micron)

The composition of the fine ash (<63 micron) of the BC Phase 2 deposits was analyzed both by XRF and SEM-EDS to investigate the presence of elements typically carried as micron-scale particles by volcanic aerosols in the eruptive cloud (e.g. Symonds et al. 1994; Moune et al. 2010). The fine ash shows a remarkable enrichment in S (up to 8 wt.% SO_3) in comparison to the composition of the juvenile clasts (Table 2). The highest values are comparable to samples of the surficial advanced argillic facies at La Fossa (Fulignati et al. 1998; Boyce et al. 2007). On the other hand, chlorine shows no enrichment. Native S and other phases like jarosite have been decteted in this fine ash. Among the trace elements analyzed, the base metals (Cu, Zn, Pb) and As are generally enriched in the fine ash in comparison to both the

juvenile lapilli and bombs in the BC. These elements are also higher in BC fine ash than in the fine ash of other products at La Fossa (Fig. 9).

Rock magnetic results

Deposition temperature of the BC

Most unaltered trachytic lava clasts (ca. 80%) in the BC belong to Type C of Cioni et al. (2004): their NRM consists of two components, the blocking temperature (T_b) spectrum of which is well defined (Figs. 10a and 10c) and the reheating temperature is well constrained within an interval of 40 °C. The T_b spectra of the low-T and high-T components overlap in ca. 16% of the clasts (Type D1 of Cioni et al., 2004). For these clasts, the reheating temperature is defined within a wider interval, which in some cases may be as wide as 200 °C (Fig. 10b). According to McClelland (1982), this feature points to the acquisition of a chemical remanent magnetization (CRM) due to alteration of ferromagnetic minerals contemporaneous with reheating. The remaining 4% of the clasts are Type A of Cioni et al. (2004). In this type, the reheating temperature is lower than the T_b spectrum and thus did not affect the primary remanence. Figure 11 shows the areal distribution of the estimated T_{dep} at each site and its vertical variation throughout the deposit at section 5, together with the reheating interval for all clasts. The T_{dep} values are in the range 200-260 °C. A higher value of 280 °C appears only at sub-site *2c*_middle, section 5 (Fig. 11).

Paleomagnetic dating of the BC eruption

Of the lithic clasts collected for the temperature measurements, thirty-eight were oriented at four sites, and used for paleomagnetic dating analyses as well. The high-T and low-T directions given by PCA analysis could therefore be referred to the geographical reference system. Twenty-three low-T directions are well defined because the strong decrease in remanence intensity during the first heating steps allows computations of a reliable best-fit line (Fig. 10a). In the remaining cases, intensity decreases little with heating and the clustering of points (Fig. 10c) results in a poorly defined fit line. Low-T directions were taken into account only when their Maximum Angular Deviation (MAD) was lower than 10 °C.

As expected, the high-T directions are broadly scattered, a result of the lithic clasts having been chaotically transported within the PDC. For these clasts, the randomness test (Watson 1956) is passed at the 95% confidence level. On the contrary, the low-T directions (Fig. 12a), acquired after deposition of the BC, cluster around a mean direction (D = 12.9°, I =

55.1°, α_{95} = 5.8°), which can be regarded as the direction of the Earth's magnetic field at the time of the eruption. To obtain the archeomagnetic age for the eruption, the mean direction from the BC clasts was first relocated to Paris using the relocation via pole method. Dating was then done using the RenDate software (Lanos et al. 2005) and the French Secular Variation (SV) curve (Gallet et al. 2002) as reference. This method uses the Bayesian statistics approach, in which the probability density obtained from the inclination and declination SV curves are combined. The method may provide more than one age interval because the Earth's magnetic field changes with time, and subsequent periods may have the same paleomagnetic direction. The age interval must thus be constrained using other elements, such as for example the stratigraphy. The result indicates, at the 95% confidence level, two possible ages, both younger than the previously reported in the literature: between 918 and 1302 AD, and between 1399 and 1604 AD (Fig. 13).

Discussion

Emplacement mechanisms of the BC

The deposits of Phase 1 consist of grey, slightly indurated ash. The constant thickness, good sorting, and areal distribution suggest a fallout mechanism for their emplacement and dispersal influenced by wind from the northwest (Fig. 3a).

Most of the BC was erupted during Phase 2. In the southern and eastern sectors, four main layers have been identified. Layers *2a*, *2b* and *2d* are confined to the southern and eastern sectors, whereas layer *2c* is radially dispersed. The massive or normally graded deposits of layer *2a* accumulated from a high-concentration PDC that was predominantly controlled by the topography. In deep gullies, layer *2a* is well-stratified (Fig. 5b, section 30b), well-sorted and grain-supported (Fig. 5b), indicative of emplacement that allowed efficient sorting and elutriation processes. Similar fines-poor layers elsewhere have been attributed to enhanced turbulence in response to extreme roughness of the substratum (e.g. Freundt and Schmincke 1985; Buesh 1992; Gurioli et al. 2007). In the case considered here, the current was locally erosive, and removed small portions of UPP or Phase 1 ash deposits from the substrate. In the southeastern and eastern sectors of La Fossa, layer *2a* shows a strong ballistic component suggestive of explosions that occurred at the beginning of this paroxysmal phase.

Layer *2b* represents sedimentation from a finer-grained and more dilute PDC in which traction processes operated (e.g. Arnott and Hand 1989; Druitt 1992). The local presence of layers *2a* and *2b* without layer *2c*, both in proximal (Supporting Material 1) and distal

locations (Fig. 5c, section 18), the lack of these two layers on the other side of the volcano (Fig. 3b), and the presence of degassing pipes that are truncated at the bottom of layer *2c* (Fig. 5c, section 49), indicate that layers *2a* and *2b* were deposited from a PDC that was separate from the current that deposited layer *2c*.

The characteristics of layer *2c* including its massive aspect, poor sorting, valley-pond morphology, grain-size variations controlled by paleotopography, reverse grading, absence of internal laminae, and the presence of a finer grained layer at the base, are consistent with sedimentation from a high-concentration PDC.

Layer *2d* can be interpreted as an ash fall deposit on the basis of its fine grained nature, good sorting and massive aspect. Dispersal was probably controlled by the main direction of the wind, this being towards the southeast. Layer *2d* lies on an erosive contact with layer *2c*, suggesting a short break between the emplacement of this massive ash and layer *2c*. However, layer *2d* lacks accretionary lapilli, has the same matrix color as other Phase 2 deposits and is separated from Phase 3 deposits by a well defined bed of UPP ash, so it is considered to be part of Phase 2.

The Phase 3 deposits are rich in accretionary lapilli and have thickness variations, sorting, and distribution consistent with fall emplacement, mainly driven by a southeastly wind. The presence of three layers suggests that at least three explosions were involved. Such activity thus characterized the last phase of the eruption.

Components involved in the BC explosive eruption

Three main features of the BC are distinctive: 1) the yellow color of Phase 2 deposits, 2) the high lithic/juvenile ratios, and 3) the high percentage of hydrothermally altered lithic clasts. These features have been described for deposits emplaced during magmatic-hydrothermal eruptions (Browne and Lawless 2001). The juvenile components are mainly confined to the coarse ash (Figs. 7 and 8), although juvenile lapilli and scattered bombs are present (Fig. 2e). The crusts on the surface underlying the BC, and the presence of abundant hydrothermally altered clasts in the BC indicate that a hydrothermal system was active at the time of the BC eruption. The pre-eruptive alteration of these clasts in the advanced argillic and silicic alteration facies, is indicative of a high-sulfidation environment, typical of a relatively shallow magma degassing (e.g. Arribas 1995; Hedenquist 1995). The same alteration facies and degassing activity characterize La Fossa today (e.g. Boyce et al. 2007) suggesting that the hydrothermal system active prior to the BC
eruption was analogous to the present system.

The presence of patinae on the fresh juvenile glass shards of Phase 2 deposits suggests the occurrence of syn- or post-depositional alteration processes. These patinae are formed by microcrystalline smectites and are similar to those described by Capaccioni et al. (1991) and Capaccioni and Coniglio (1995) at Vulcano in the "wet surge" deposits of La Fossa. The high percentage of clasts altered under low pH conditions suggests that acidic hydrothermal fluids, hosted in the altered rocks of the conduit, were available at the moment of the eruption and afterwards. We exclude the long-term presence of acidic gas and/or groundwater circulating through permeable layers in the entire La Fossa section as the cause, because only Phase 2 deposits have been affected and therefore the alteration was syn-depositional.

The presence of native S and also other phases like jarosite, in the fine ash of Phase 2 deposits explains their yellow color and suggests that the finest fraction is largely composed of S-rich hydrothermally altered fragments. The sulfur may have come from the condensation of magmatic sulfur species in the eruptive cloud (e.g. Varekamp et al. 1986). Even though La Fossa magmas have low sulfur contents, S degassing from a deep magmatic system has been demonstrated by melt inclusions studies (Clocchiatti et al. 1994). Degassing was very likely strong before the BC eruption, as suggested by the presence of the hydrothermal system that was responsible for the high content of altered lithic clasts in the BC.

The fine ash has higher Pb, Cu, Zn, and As abundance than the juvenile lapilli and bombs of Phase 2 deposits and the superficial hydrothermally altered rocks and the fine ash of other products of La Fossa (Fig. 9) suggesting that the BC formed in the presence of an anomalously high amount of metals. These metals typically partition into magmatic-hydrothermal fluids (e.g. Robb 2005) that may have been released during the eruption. The eruptive plumes of several volcanoes have been observed to carry remarkable amounts of Zn, Cu, Au, Pb, Cd, Cl, Br, Se, Sb, Hg, Ir, As, and S (Lepel et al. 1978; Zoller et al. 1983; Varekamp et al. 1986; Hedenquist 1995). These elements are carried by chloride- and sulfate-bearing microcrystals (Varekamp et al. 1986; Ammann et al. 1993). Therefore, the enrichment in Pb, Cu, Zn, and As in the <63 micron fraction of the BC may be accomplished by means of micron-sized particles carrying these trace elements, which were adsorbed onto the volcanic ash.

The temperature of the PDC deposits

According to the rock magnetic measurements, the Phase 2 deposits had a T_{dep} of 200-260 °C. These values could represent the T_{dep} of the BC as well as secondary processes, such as viscous remanent magnetization (VRM) or post-eruptive heating and hydrothermal alteration.

The VRM hypothesis can be tested using the approximate relationship between unblocking temperature (T_{ub}) and time (Bardot and McClelland 2000), $T_{ub} = 75 + 15 \log(t)$, where t is the time the magnetic domains need to stay at temperature T_{ub} to unblock and remagnetize according to the present field. The BC eruption occurred in the Middle Ages, which suggests T_{ub} ~ 120-125 °C, well below the minimum value of 200 °C estimated for the deposition temperature. The VRM hypothesis is therefore discarded.

Hydrothermal and fumarolic activities are present in the La Fossa edifice and might well have operated since the BC eruption. Three arguments, however, indicate that these phenomena have not affected the remanence record:

1) special attention was paid to collect unaltered trachytic lava clasts;

2) the estimated T_{dep} values are uniform all over La Fossa;

3) the natural remanent magnetization of all lithic clasts consists only of two components. If the low-T component is related to post-eruption processes, the thermal overprint due to the reheating by the PDC deposits should appear as a third, intermediate temperature component, unless T_{dep} was high enough to completely erase the clasts' primary remanences; that would require a temperature higher than 540-560 °C.

In conclusion, we can reasonably regard the temperature values (Fig. 11) as the actual T_{dep} values of the Phase 2 deposits.

The age of the BC eruption

The UPP ash from Lipari is interbedded with the BC, and the two units have been therefore regarded as coeval (e.g. Cortese et al., 1986). The UPP at Lipari is younger than the sixth century AD, based on the ^{14}C age (1220 +/- 100 years before 1950) of an underlying paleosol (Keller 1970). The UPP ash underlies the obsidian lavas of Rocche Rosse at Lipari. The stratigraphic constraints show that the BC eruption is older than Rocche Rosse; on the other hand, the two eruptions occurred in a very short time span, because their paleomagnetic directions are statistically indistinguishable (Fig. 12b). The archaeomagnetic age of Rocche Rosse, based both on direction (D = 14.5°, I = 50.6°, α_{95} = 6.1°, Zanella 2006) and paleointensity (52.4 +/- 1.1 μT, Leonhardt et al. 2006) and derived using the Regional Cap Harmonic Analysis Technique (Pavón-Carrasco 2009) is 1054 – 1205 AD at the 95% confidence limit (Pavón-Carrasco, personal communication). The younger of the two possible archaeomagnetic ages of BC (1399 – 1604 AD) is thus not tenable, whereas the older (918 – 1302 AD) is consistent with the Rocche Rosse age. In conclusion, taking into account the

Rocche Rosse age, an age around 1000 – 1200 AD may be reasonably inferred for the BC eruption.

Conclusions

During the BC eruption, 0.002 km^3 of lithic-rich deposits were dispersed essentially by PDC and subordinate fallout around La Fossa cone and on the floor and walls of the La Fossa caldera depression. The opening phase of the eruption, Phase 1, deposited a fine ash layer with a north-westerly dispersal. One, or several, explosions occurred at the beginning of the paroxysmal phase of the eruption, Phase 2, and produced ballistic blocks and impact sag structures. This phase was characterized by the emplacement of narrowly dispersed lithic-rich, stratified PDC deposits (layers *2a* and *2b*), followed by a radially distributed, topographically controlled, coarse-grained PDC deposit (layer *2c*), and fallout from an ash cloud (layer *2d*). Phase 3 involved at least three explosions and generated accretionary lapilli-rich ash fall deposits.

The magma involved in the BC eruption was mainly rhyolitic to trachytic in composition, though only a small fraction of magma was erupted. The prevalence of hydrothermally altered lithic clasts with respect to juvenile clasts and the syn-depositional alteration suggest that the eruption involved an active hydrothermal system. The homogeneous, relatively low T_{dep} of the PDC deposit, may reflect the temperature of the hydrothermal fluids, rather than a magmatic temperature. As observed for other volcanoes (e.g. Cavache and Williams 1992), these lithic-rich PDC deposits, have extents similar to those of pumice-rich PDC deposits (e.g. Gurioli et al. 2010) and have a lethal temperature, as we found in this study.

The most explosive eruption expected at La Fossa has been predicted to result from magma-water interaction (Barberi et al. 1991; Frazzetta and La Volpe 1991; Dellino et al. 2011) or a magma-hydrothermal system interaction (Dellino 1997). Because a hydrothermal system, linked to degassing of a shallow magmatic system, is currently active at La Fossa, we believe that a BC-type eruption must be considered as a likely eruption scenario for Vulcano.

Acknowledgement

The authors are grateful to P. Dellino and L. La Volpe for numerous field discussions both on the BC and on La Fossa stratigraphy in general. S. Marchetti is thanked for her great work

done in 1992-1993 as part of her undergraduate thesis. Thanks to A. Freundt and two anonymous reviewers for their formal review on an early version of this manuscript, and to R. Cioni, B. Houghton and A. Harris for informal reviews of the draft of the revised manuscript. A special thank you to A. Freundt, who agreed to review the paper again and made great corrections. Thanks to L. Morgan and L. Mastin for all their advice that greatly improved this manuscript. We are extremely grateful to the editor, J McPhie, for her patience and hard work in getting this manuscript into shape. M. Menichini helped with X-ray fluorescence analysis and F. Colarieti with SEM-EDS (both DST, University of Pisa), and L. Bagnasco performed rock magnetic measurements (University of Turin). This research was supported by a CNR-GNV grant to A. Sbrana for volcanic hazard assessment at Vulcano and by the INGV-DPC Project 2004-2006 (V3_5-Vulcano, Task 1: Eruptive products, eruptive scenarios and hazard, P.I. G. De Astis). This is Laboratory of excellence *ClerVolc* contribution n° 17.

References

Ammann CM, Meehl GA, Washington WM, Zender CS (2003) A monthly and latitudinally varying volcanic forcing dataset in simulations of 20th century climate. Geophys Res Lett, 30, doi:10.1029/2003GL016875

Arnott RWC, Hand BM (1989) Bed forms, primary stuctures on grain fabric in the presence of suspended sediment rain. J Sed Petrol 59:1062-1069

Arribas Jr A (1995) Characteristics of high-sulfidation epithermal deposits, and their relation to magmatic fluid. In: Thompson JFH (Ed.), Magmas Fluids and Ore Deposits, vol. 23. Mineralogical Association of Canada Short Course, pp. 419–454

Arrighi S, Tanguy JC, Rosi M (2006) Eruptions of the last 2200 years at Vulcano and Vulcanello (Aeolian Islands, Italy) dated by high accuracy archeomagnetism. Phys Earth Planet Int, doi:10.1016/j.pepi.2006.07.010

Barberi F, Cioni R, Rosi M, Santacroce R, Sbrana A, Vecci R (1989) Magmatic and phreatomagmatic phases in explosive eruptions of Vesuvius as deduced by grain-size and compositional analysis of pyroclastic deposits. J Volcanol Geotherm Res 38:287–307

Barberi F, Neri G, Valenza M, Villari L (1991) 1987-1990 unrest at Vulcano. Acta Vulcanol 1:269-276

Barberi F, Gandino A, Gioncada A, La Torre P, Sbrana A, Zenucchini C (1994) The deep structure of the Eolian arc (Filicudi–Panarea–Vulcano sector) in light of gravity, magnetic and volcanological data. J Volcanol Geotherm Res 61:189-206

Bardot L, McClelland E (2000) The reliability of emplacement temperature estimates using palaeomagnetic methods: a case study from Santorini, Greece. Geophys J Int 143:39-51

Bigazzi G, Bonadonna F (1973) Fission track dating of the obsidian of Lipari Island (Italy). Nature 242:322-323

Boyce AJ, Fulignati P, Sbrana A, Fallick AE (2007) Fluids in early stage hydrothermal alteration of high-sulfidation epithermal systems: A view from the Vulcano active hydrothermal system (Aeolian Islands, Italy). J Volcanol Geotherm Res 166:76-90

Browne PRL, Lawless JV (2001) Characteristics of hydrothermal eruptions, with examples from New Zealand and elsewhere. Earth Sci Rev 52:299-331

Buesh DC (1992) Incorporation and redistribution of locally derived lithic fragments within a pyroclastic flow. Geol Soc Am Bull 104:1193-1207

Calvache MR, Williams SN (1992) Lithic-dominated pyroclastic flows at Galeras Volcano, Colombia-An unrecognizied volcanic hazard. Geology 20:539-542

Capaccioni B, Coniglio S, Fratini F (1991) Clay minerals on recent products of hydromagmatic activity: considerations on their genesis. Acta Vulcanol 1:69-77

Capaccioni B, Coniglio S (1995) Varicolored and vesiculated tuffs from La Fossa volcano, Vulcano Island (Aeolian Archipelago, Italy): evidence of syndepositional alteration processes. Bull Volcanol 57:61–70

Cas RAF, Wright JV (1987) Volcanic successions. Chapman & Hall, London, 528 pp

Chiodini G, Cioni R, Marini L, Panichi C (1995) Origin of the fumarolic fluids of Vulcano Island, Italy and implications for volcanic surveillance. Bull Volcanol 57(2):99-110

Chough SK, Sohn YK (1990) Depositional mechanics and sequences of base surges, Songaksan tuff ring, Cheju Island, Korea. Sedimentology 37:1115–1135

Cioni R, Gurioli L, Lanza R, Zanella E (2004) Temperatures of the AD 79 pyroclastic density current deposits (Vesuvius, Italy). J Geophys Res 109, B02207, doi:10.1029/2002JB002251

Clocchiatti R, Gioncada A, Mosbah M, Sbrana A (1994) Possible deep origin of sulfur output at Vulcano, Southern Italy. in the light of melt inclusion studies. Acta Vulcanol 5:49–53

Cortese M, Frazzetta G, La Volpe L (1986) Volcanic history of Lipari (Aeolian Islands) in the last 10.000 years. J Volcanol Geoth Res 27:117-133

De Astis G, Frazzetta G, La Volpe L (1989) I depositi di riempimento della Caldera del Piano e i depositi della Lentia. Boll GNV 2:763–778

De Astis G, Dellino P, La Volpe L, Lucchi F, Tranne CA (2006). Geological map of the Vulcano Island. La Volpe L, De Astis G (eds), printed by Litografia Artistica Cartografica (LAC), Firenze Italy

Dellino P (1997) Scenario eruttivo ed eruzione massima attesa. Progetto Vulcano, Risultati delle Attività di ricerca 1993-1995, Felici Editore

Dellino P, La Volpe L (1997) Stratigrafia, dinamiche eruttive e deposizionali, scenario eruttivo e valutazioni di pericolosità a La Fossa di Vulcano. Progetto Vulcano, Risultati delle Attività di ricerca 1993-1995, Felici Editore

Dellino P, De Astis G, La Volpe L, Mele D, Sulpizio R (2011) Quantitative hazard assessment of phreatomagmatic eruptions at Vulcano (Aeolian Islands, Southern Italy) as obtained by combining stratigraphy, event statistics and physical modeling. J Volcanol Geoth Res 201:364-384

Druitt TH (1992) Emplacement of the 18 May 1980 lateral blast deposits ENE of Mount St. Helens, Washington. Bull Volcanol 54:554-572

Folk RL, Ward WC (1957) Brazos river bar: a study in the significance of grain-size parameters. J Sed Petrol 27:3-26

Franzini M, Leoni L, Saitta M (1975) Revisione di una metodologia analitica per fluorescenza-X basata sulla correzione completa sugli effetti di matrice. Rend Soc It Mineral Petrol 31:365-378

Frazzetta G, La Volpe L, Sheridan MF (1983) Evolution of the Fossa cone. J Vulcanol Geotherm Res 17:329-360

Frazzetta G, Gillot PY, La Volpe L, Sheridan MF (1984) Volcanic hazards at Fossa of Vulcano: data from the last 6,000 years. Bull Volcanol 47:105-124

Frazzetta G, La Volpe L (1991) Volcanic history and maximum expected eruption at "La Fossa di Vulcano" (Aeolian Islands, Italy). Acta Vulcanol 1:107-114

Freundt A, Schmincke HU (1985) Lithic-enriched segregation bodies in pyroclastic flow deposits of Laacher See Volcano (East Eifel, Germany). J Geol 25:193-224

Fulignati P, Gioncada A, Sbrana A (1998) Geologic model of the magmatic-hydrothermal system of Vulcano (Aeolian Island Italy). Mineral Petrol 62:195-222

Fulignati P, Gioncada A, Sbrana A (1999) Rare-earth element (REE) behaviour in the alteration facies of the active magmatic-hydrothermal system of Vulcano (Aeolian Islands Italy). J Volcanol Geotherm Res 88:325–342

Fulignati P, Sbrana A, Luperini W, Greco V (2002) Formation of rock coatings induced by the acid fumarole plume of the passively degassing volcano of La Fossa (Vulcano Island, Italy). J Volcanol Geotherm Res 115:397-410

Gallet Y, Genevey A, Le Goff M (2002). Three millennia of directional variation of the Earth's magnetic field in Western Europe as revealed by archaeological artefacts. Phys Earth Planet Int 131:81-89

Gioncada A (1997) L'attività eruttiva degli ultimi 50000 anni di Vulcano (Eolie): aspetti vulcanologici e magmatologici". Tesi di Dottorato, Università degli Studi di Pisa.

Gioncada A, Sbrana A (1991) La Fossa Caldera, Vulcano: inferences from deep drillings. Acta Vulcanol 1:115–126

Gioncada A, Gurioli L, Sbrana A (1995) The hydrothermal-magmatic eruption of Breccia di Commenda. Per Miner 64:191-192

Gioncada A, Sbrana A, Bottazzi P, Clocchiatti R, Del Moro A, Joron JL, Ottolini L, Pinarelli L (1997) Il sistema di alimentazione di La Fossa. Progetto Vulcano, Risultati delle Attività di ricerca 1993-1995, Felici Editore

Gioncada A, Clocchiatti R, Sbrana A, Bottazzi P, Massare D, Ottolini L (1998) A study of melt inclusions at Vulcano (Aeolian islands, Italy): insight on the primitive magmas and on the volcanic feeding system. Bull Volcanol 60:286–306

Gurioli L (1994) Studio vulcanologico dell'eruzione della breccia di Commenda e considerazioni stratigrafiche sul ciclo di Commenda e sulla sequenza basale del cilo di Pietre otte. Tesi di Laura, Università di Pisa

Gurioli L, Sbrana A (1999) Caratterizzazione stratigrafica e sedimentologica dei depositi dell'eruzione della Breccia di Commenda (Isola di Vulcano) con particolare riferimento ai depositi di flusso piroclastico ricchi in litici relativi alla fase parossistica dell'eruzione. Atti Soc Tosc Sci Nat Mem 106:103-112

Gurioli L, Zanella E, Pareschi MT, Lanza R (2007) Influences of urban fabric on pyroclastic density currents at Pompeii (Italy), part I: flow direction and deposition. J Geophys Res 112: 721 BOS213

Gurioli L, Sulpizio R, Cioni R, Sbrana A, Luperini W, Santacroce R, Andronico D (2010) Pyroclastic flow hazard assessment at Somma-Vesuvius based on the geological record. Bull Volcanol, DOI:10.1007/s00445-010-0379-2

Hedenquist JW (1995) The ascent of magmatic fluid: discharge versus mineralization. In: Thompson JFH (Ed), Magmas Fluids and Ore Deposits, vol 23. Mineralogical Association of Canada Short Course, pp. 263–289

Inman DL (1952) Measures for describing the size distribution of sediments. J Sed Petrol 22:125-145

Keam RF (1988) Tarawera. Privately published by the author, 472 pp., ISBN 0-473-00444-5

Keller J (1970) Datierung der obsidiane und bimstuffe von Lipari, N Jb Geol Mh, 90-101

Keller J (1980) The Island of Vulcano. Rend Soc Ital Min Petrol 36:369-414

Kirschvink JL (1980) The least-squares line and plane and the analysis of palaeomagnetic data. Geophys J Roy Astron Soc 62:699-718

Lanos P, Le Goff M, Kovacheva M, Schnepp E (2005) Hierarchical modelling of archaeomagnetic data and curve estimation by moving average technique. Geophys J Int 160:440-476

Leonhardt L, Matzka J, Nichols ARL, Dingwell DB (2006) Cooling rate correction of paleointensity determination for volcanic glasses by relaxation geospeedometry. Earth Planet Sci Lett 243:282-292

Lepel E, Stefansson K, Zoller W (1978) The enrichment of volatile elements in the atmosphere by volcanic activity: Angustine Volcano 1976. J Geophys Res 83:6213-6220

Lucchi F, Tranne CA, Calanchi N, Pirazzoli P, Romagnoli C, Radtke U, Reyss JL, Rossi PL (2004) Stratigraphic constraints to date late Quaternary ancient shorelines and to evaluate

vertical movements at Lipari (Aeolian Islands): Quaternary International 115/116, 105–115, doi: 10.1016/S1040-6182(03)00100-9

Malin MC, Dzurisin D, Sharp RP (1983) Stripping of Keanakakoi tephra on Kilaua Volcano, Hawaii. Geol Soc Am Bull 94:1148-1158

Mastin LG (1991) The roles of magma and groundwater in the phreatic eruptions at Inyo Craters, Long Valley Caldera, California. Bull Volcanol 57:85–98

McClelland EA (1982) Discrimination of TRM and CRM by blocking-temperature spectrum analysis. Phys Earth Planet Int 30:405-414

McClelland EA, Druitt TH (1989) Palaeomagnetic estimate of emplacement temperatures of pyroclastic deposits on Santorini, Greece. Bull Volcanol 51:16–27

McFadden PL, Lowes FJ (1981) The discrimination of mean directions drawn from Fisher distribution. Geophys J Roy Astr Soc 67:19-33

Moune S, Gauthier PJ, Delmelle P (2010) Trace elements in the particulate phase of the plume of Masaya Volcano, Nicaragua. J Volcanol Geothermal Res 193:232-244

Naughton JJ, Greenberg VA, Gognel R (1976) Incrustations and fumarolic condensates at Kilauea. J Volcanol Geothermal Res 1:141-165

Pavón-Carrasco FJ, Osete ML, Torta JM, Gaya-Piqué LR (2009) A regional archeomagnetic model for Europe for the last 3000 years, SCHA.DIF.3K: Applications to archeomagnetic dating. Geochem Geophys Geosyst 10, Q03013, doi:10.1029/2008GC002244

Robb L (2005) Introduction to ore-forming processes. Blackwell Publishing, pp. 373.

Scott AC, Sparks RS, Bull ID, Knicker H, Evershed RP (2008) Temperature proxy data and their significance for the understanding of pyroclastic density currents. Geology 36:143-146

Sheridan MF (1980) Pyroclastic block flow from the September 1976, eruption of La

Soufrière volcano, Guadalupe. Bull Volcanol 43:397-402

Simmons SF, Keywood M, Scott BJ, Keam RF (1993) Irreversible change of the Rotomahana–Waimangu hydrothermal system (New Zealand) as a consequence of a volcanic eruption. Geology 21:643-646

Sohn YK, Chough SK (1989) Depositional processes of the Suwolbong tuff ring, Cheju Island (Korea). Sedimentology 36:837–855

Soligo M, De Astis G, Delitala MC, La Volpe L, Taddeucci A, Tuccimei P (2000) Uranium-series disequilibria in the products from Vulcano Island (Sicily, Italy): isotopic chronology and magmatological implications. Acta Vulcanologica 12:49-59

Symonds RB, Rose WI, Bluth GJS, Gerlach TM (1994) Volcanic gas studies: methods, results and applications. In: Carroll MR, Holloway JR (Eds.),Volatiles in Magmas: Rev Mineral, Mineral Soc Am, pp. 1-66

Tanguy JC, Le Goff M, Principe C, Arrighi S, Chillemi V, Paiotti A, La Delfa S, Patanè G (2003) Archaeomagnetic dating of Mediterranean volcanics of the last 2100 years: validity and limits. Earth Planet Sci Lett 211:111-124

Van Der Plas L, Tobi AC (1965) A chart for judging the reliability of point counting results. Am J Sci 263:87-90

Varekamp JC, Thomas E, Germani M, Buseck PR (1986) Particle chemistry of the volcanic plumes of Mt. Etna and Mt. St. Helens. J Geophys Res 91:B12, 12,233-12,248

Ventura G (1994) Tectonics, structural evolution and caldera formation on Vulcano Island (Aeolian Archipelago, southern Tyrrheanian Sea). J Volc Geotherm Res 60:207-224

Watson GS (1956) A test for randomness of directions. Mon Not Roy Astron Soc Geophys Supp 7:160–161

Wohletz K, Heiken G (1992) Volcanology and Geothermal Energy. Univ. California Press,

432 pp

Zanella E (2006) Magnetic chronology in recent volcanic rocks: basic principles and case histories from Aeolian Islands. Acta Vulcanologica 18:35-46

Zanella E, Gurioli L, Pareschi MT, Lanza R (2007). Influences of urban fabric on pyroclastic density currents at Pompeii (Italy): 2. Temperature of the deposits and hazard implications. J Geophys Res 112, B05214, doi:10.1029/2006JB004775

Zanella E, Gurioli L, Lanza R, Sulpizio R, Bontempi M (2008) Deposition temperature of the Ad 472 Pollena pyroclastic density current deposits, Somma-Vesuvius, Italy. Bull Volcanol, DOI 10.1007/s00445-008-0199-9

Zijderveld JDA (1967) Analysis of results. In: Collinson DW, Creer KM, Runcorn SK (eds) Methods in palaeomagnetism. Elsevier Sci, New York, pp 254–286

Zoller WH, Parrington JR, Phelan Kotra JM (1983) Iridium enrichment in airborne particles from Kilauea volcano: January 1983. Science 222:1118–1121

Figure captions

Fig. 1 a) Shaded relief map of La Fossa di Vulcano. White dots, studied sections; black dots, sections sampled for rock magnetic measurements. b) Composite stratigraphic section of La Fossa cone from De Astis et al. (2006). The thickness is not to scale.

Fig. 2 a) Composite stratigraphic section of the "Breccia di Commenda" (BC). Thickness on the left in cm. UPP * = Upper Pilato Pumice. The letters refer to the different layers observed in the deposits of Phase 2 in the southern and eastern sectors. b) The BC at section 5 (black dots, samples for rock magnetic measurement). c) Phase 1 deposits and layers *2a* and *2b* in section 5 in the eastern sector. d) Layer 2*d* and Phase 3 deposits in the eastern sector. e) Ballistic bomb in Layer 2*a* in the Caruggi area. f) Red layer *2c* in the western sector. See Figure 1 for the location of the sections.

Fig. 3 Dispersal of the BC. a) Isopachs of Phase 1 ash. b) Dispersal of Phase 2 deposits; dark

grey area, layers *2a+2b+2c*; pale grey area, layer *2c*. c) Isopachs of Phase 3 deposits. Isopachs in cm. Black dots, studied sections.

Fig. 4 Three-component grain-size variations of the BC, Mdϕ (Median Diameter) versus σϕ (sorting), and lateral facies variations in Phase 2 deposits related to the topography. Coarse lapilli are between 16-64 mm in diameter and lapilli are between 16-2 mm in diameter.

Fig. 5 Lateral and vertical facies variations and grain size data for Phase 2 deposits. a) Palizzi area (sections 5 and 3). b) Gully east of Palizzi lava (sections 45, 30b and 30a). c) Caruggi area (sections 49 and 19). See Figure 1 for section locations. *2a, 2b, 2c*, and *2d* refer to the four layers of Phase 2 described in the text. Grain size analyses of sampled layers were performed at half-phi intervals. Graphs show wt.% versus grain size in phi. In Figure 5a, section 3, the weight percentage scale is logarithmic to account for the coarse-grained fragments (up to 256 mm), weighed in the field.

Fig. 6 a) Rhyolitic and trachytic juvenile fragments from the coarse ash of Phase 2, layer *2c*. b) SiO_2 wt.% of juvenile glass fragments in coarse ash in Phase 2 deposits. Data for 41 juvenile coarse ash clasts are shown. Each datum is the mean of at least three analyses on each clast by microprobe. The symbols show the composition of the glass in the three clasts in (a).

Fig. 7 Vertical variations in components of the BC: Phase 1 sample (section 7), layer *2a* samples (section 30b), layer *2b* and fine grained facies *2c* samples (section 30a), layer *2c* from base to top (section 5), Phase 3 sample (section 9). See Figure 1 for section locations.

Fig. 8 Lateral variation in the components of layers *2a*, *2b* and *2c*. Legend in Figure 7.

Fig. 9 Cu, Zn, Pb, and As contents in the fine ash fraction (oblique dashes) and in coarse juvenile components (dark gray) of the BC, compared with the amount of the same metals in the La Fossa juvenile clasts (vertical dashes) and fine ash (white), and in the surficial altered rocks (pale gray, data from Boyce et al. 2007). All bulk analyses.

Fig. 10 Zijderveld diagrams of thermal demagnetization. Symbols: full/open dot, declination/apparent inclination; blue/red line, LT/HT best-fit line; figures, temperature

values. Specimens from a) section 12, b) section 31, c) section C3.

Fig. 11 Estimated T_{dep} for BC: a) areal and b) vertical distribution of sampling sites. For each site, the reheating range of the clasts, the overlapping diagrams (Cioni et al. 2004), and the estimated T_{dep} range are shown.

Fig. 12 Equal-area projection of: a) low-T secondary directions (dots) and mean direction (star) with Fisher's 95% ellipse of confidence limit; b) paleomagnetic directions of Commenda (dot) and Rocche Rosse (square) and associated 95% ellipses of confidence.

Fig. 13 Magnetic dating of Breccia di Commenda. The Lanos's (2005) method is applied to the French SV curve (Gallet et al. 2002), drawn together with its 95% error envelope determined by Bayesian statistics. a) Declination. b) Inclination. c) Combination of D and I distributions.

Table captions

Table 1 Representative analyses of the chemical composition of the juvenile fraction in the BC, comprising XRF analyses of unaltered lapilli and bombs, microprobe analyses of glass in juvenile bombs, microprobe analyses of glass in juvenile coarse ash in the trachyte-to-rhyolite compositional range, as well as microprobe analyses of juvenile fragments in the UPP ash.

Table 2 Mean contents in Cu, Zn, Pb, As and S in the juvenile lapilli, bombs and fine ash of the BC, compared with mean values for La Fossa pyroclastic rocks (computed from representative analyses of latitic to rhyolitic products of Grotte dei Palizzi, Pietre Cotte and Gran Cratere formations).

Supporting Material 1 Grain size and thickness data of the BC. Symbols: Section, studied log; Phase, phase of the BC eruption (Fig. 2a); Sample, collected samples; Bed_t, bed thickness variation; LM, maximum lithic clast diameter; Φ5 up to Φ95, percentile; Mz, mean diameter, from Folk and Ward (1957); Md_Φ, mean diameter and σ_Φ, sorting, from Inman (1952); F1, weight percentage of fractions finer than 1 mm; F2, weight percentage of fractions finer than 1/16 mm; L, weight percentage of lapilli; CA, weight percentage of coarse ash; J, juvenile clasts; C, crystals; Li, lithic clasts; Hydro, Hydrothermally altered clasts; Trachy, Trachytic

lava clasts; Flow, Flow banded recrystallized rhyolites ; Sub, Subvolcanic latites and trachytes.

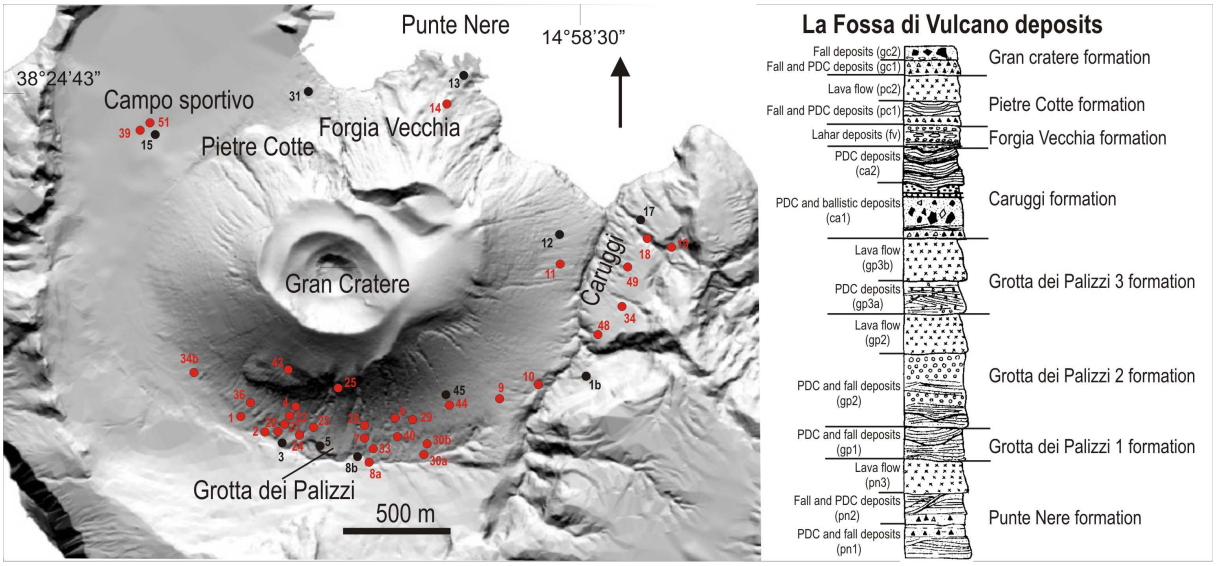
Punte Nere
14°58'30"
38°24'43"
Campo sportivo
Forgia Vecchia
Pietre Cotte
Gran Cratere
Caruggi
Grotta dei Palizzi
500 m
La Fossa di Vulcano deposits
Fall deposits (gc2)
Fall and PDC deposits (gc1)
Gran cratere formation
Lava flow (pc2)
Fall and PDC deposits (pc1)
Pietre Cotte formation
Lahar deposits (fv)
Forgia Vecchia formation
PDC deposits (ca2)
PDC and ballistic deposits (ca1)
Caruggi formation
Lava flow (gp3b)
PDC deposits (gp3a)
Grotta dei Palizzi 3 formation
Lava flow (gp2)
PDC and fall deposits (gp2)
Grotta dei Palizzi 2 formation
PDC and fall deposits (gp1)
Grotta dei Palizzi 1 formation
Lava flow (pn3)
Fall and PDC deposits (pn2)
PDC and fall deposits (pn1)
Punte Nere formation

Fig.1

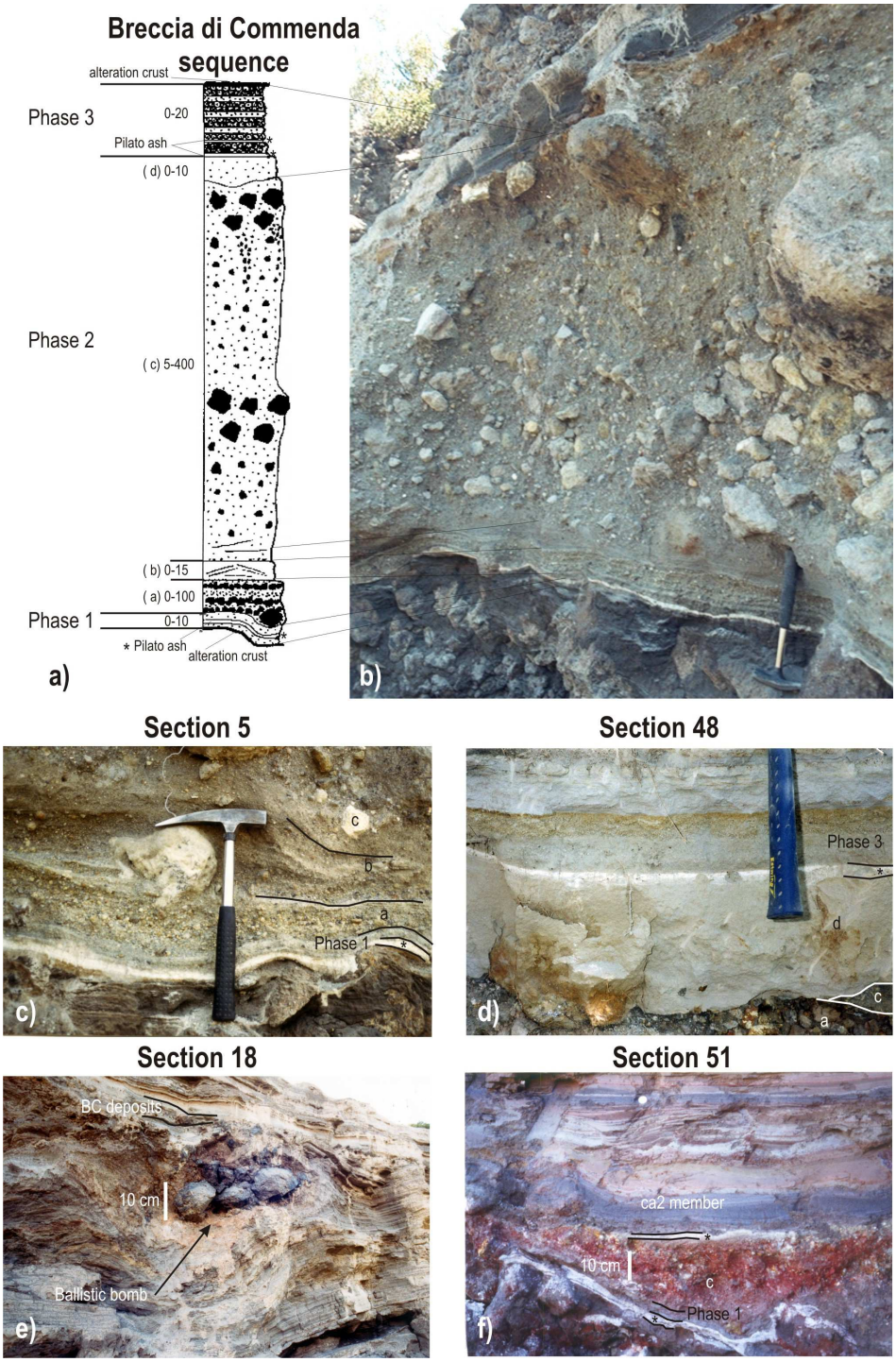
Breccia di Commenda sequence
alteration crust
Phase 3
0-20
Pilato ash
(d) 0-10
Phase 2
(c) 5-400
(b) 0-15
(a) 0-100
Phase 1
0-10
* Pilato ash
alteration crust
a)
b)
Section 5
c
b
a
Phase 1
c)
Section 48
Phase 3
d
c
a
d)
Section 18
BC deposits
10 cm
Ballistic bomb
e)
Section 51
ca2 member
10 cm
c
Phase 1
f)

Fig.2

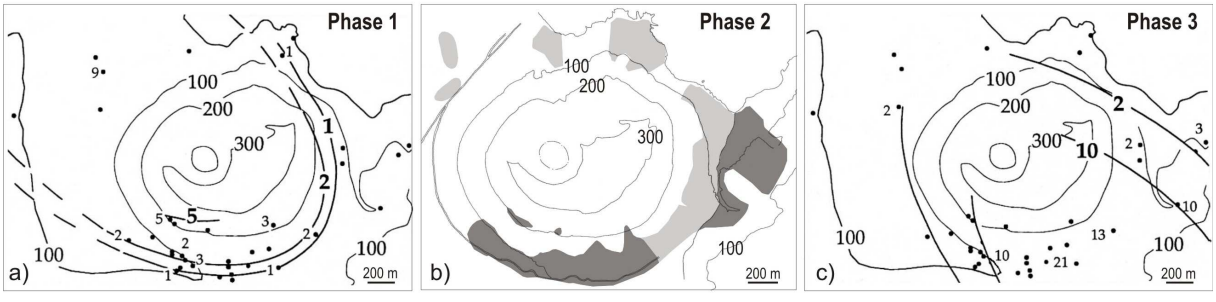
Phase 1
100
200
300
1
2
5
3
a)
200 m
Phase 2
100
200
300
b)
200 m
Phase 3
100
200
300
2
10
3
13
21
c)
200 m

Fig.3

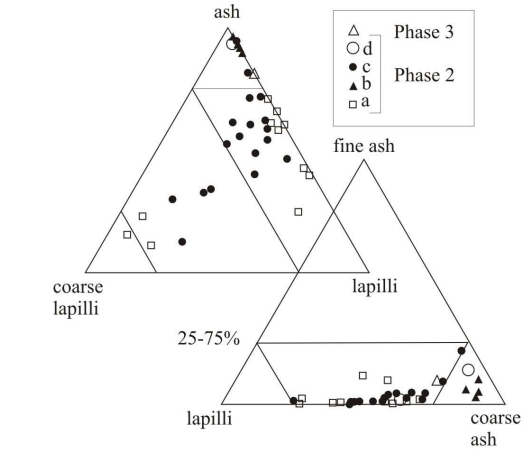

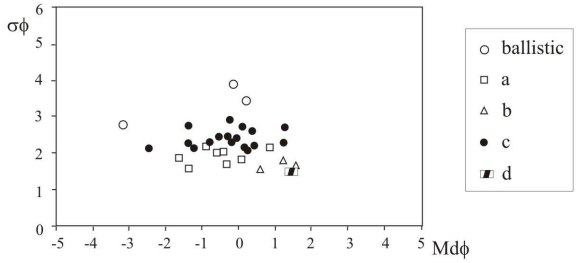

Sedimentary facies

Layers		>75% coarse lapilli (breccia)	25-75% coarse lapill and lapilli (tuff breccia)	25-75% lapilli and ash (lapilli tuff)	>75% ash (tuff)
massive to crudely stratified	a				
laminated to low angle cross laminated	b				
massive to reversely graded	c				
massive ash with accretionary	d				

Lateral facies variations

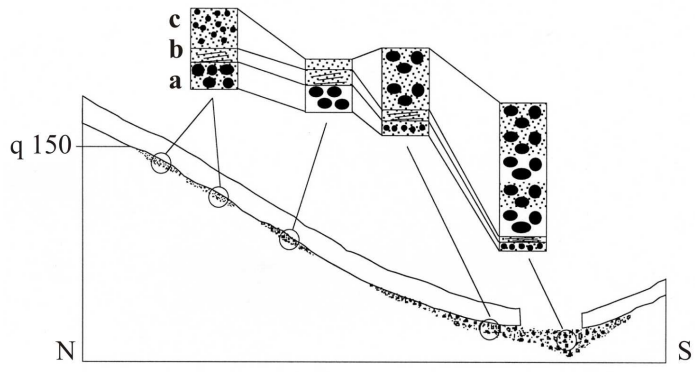

Fig.4

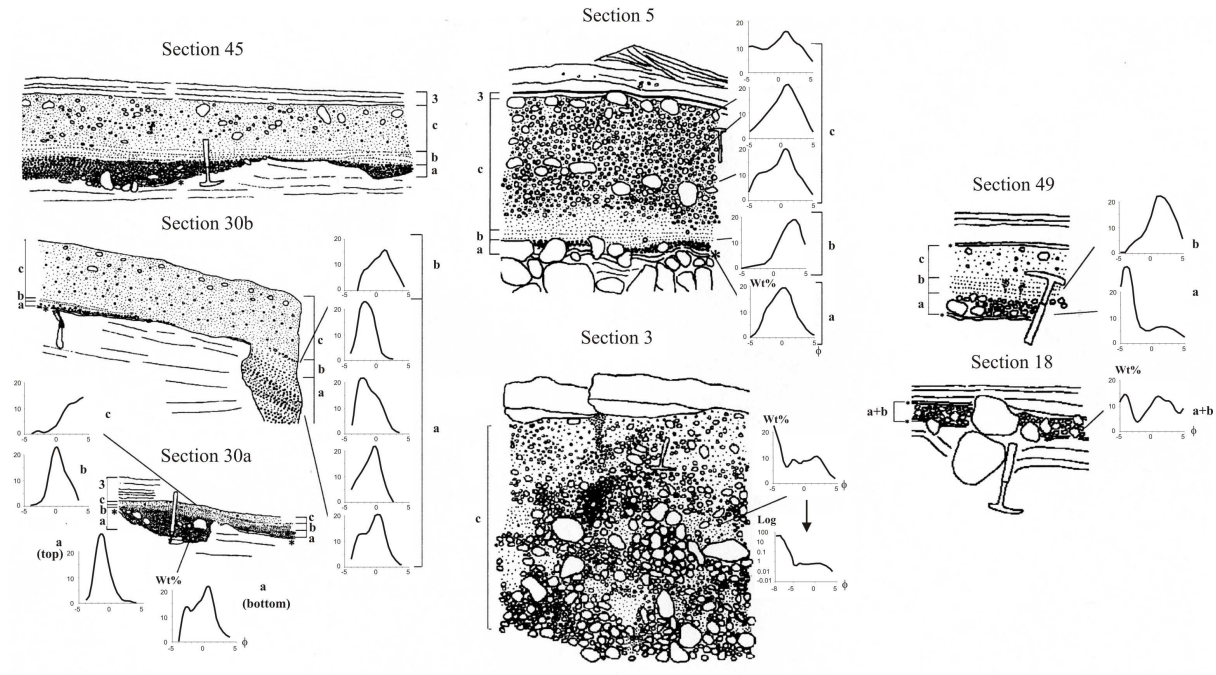
Section 45
Section 30b
Section 30a
Section 5
Section 3
Section 49
Section 18
Wt%
Log
a (top)
a (bottom)
a+b

Fig.5

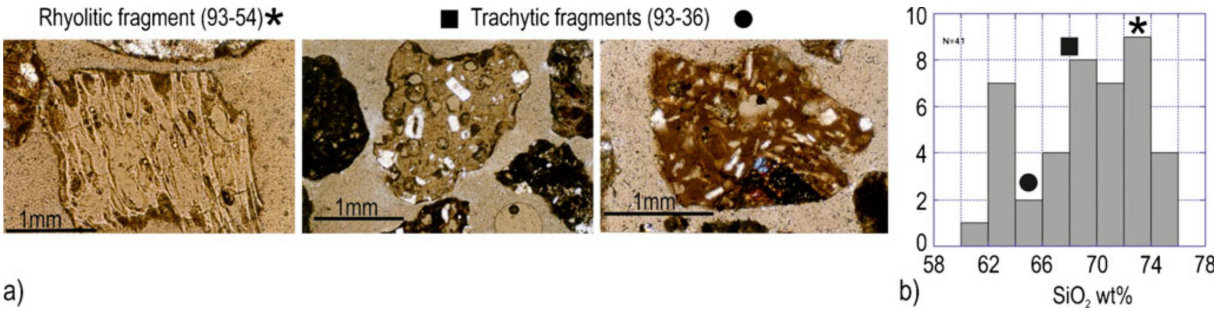
Rhyolitic fragment (93-54)*
Trachytic fragments (93-36)
1mm
1mm
1mm
a)
b)
SiO2 wt%

Fig.6

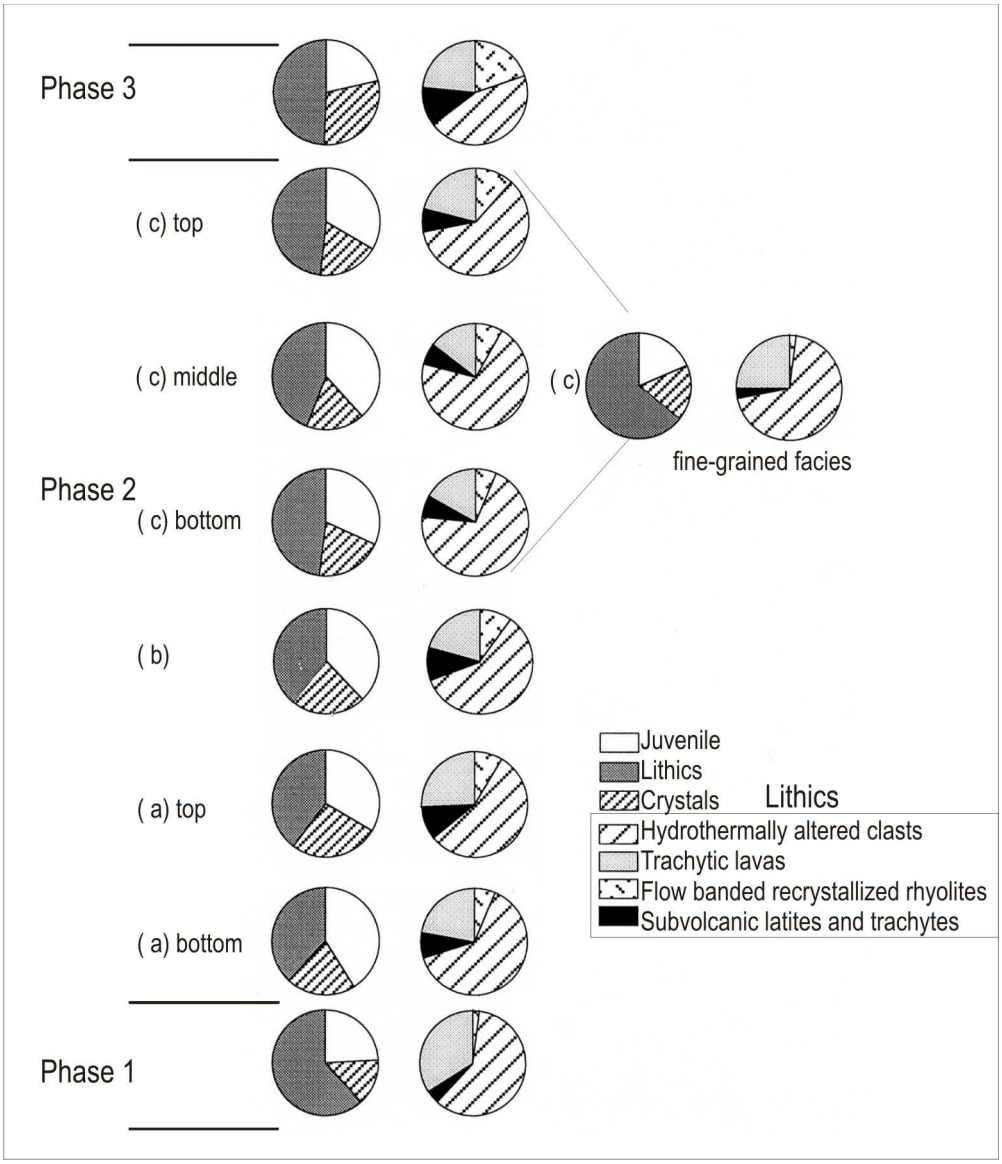
Phase 3
(c) top
(c) middle
(c)
fine-grained facies
Phase 2
(c) bottom
(b)
(a) top
(a) bottom
Phase 1
Juvenile
Lithics
Crystals
Lithics
Hydrothermally altered clasts
Trachytic lavas
Flow banded recrystallized rhyolites
Subvolcanic latites and trachytes

Fig.7

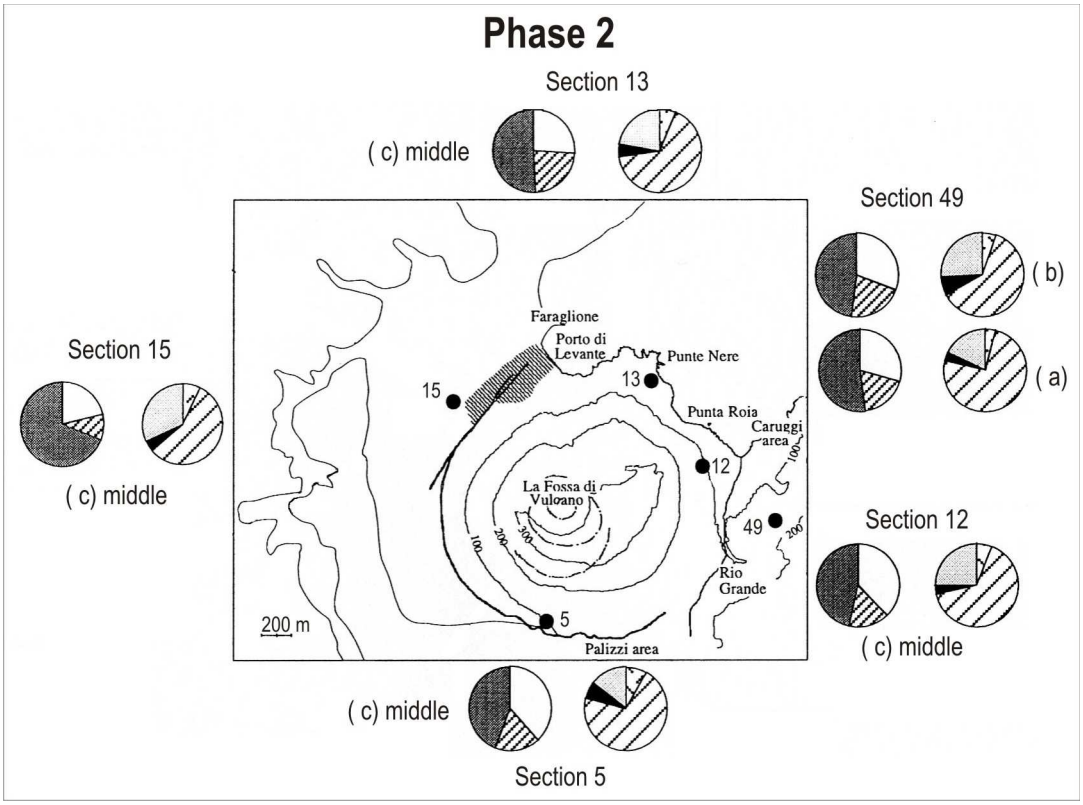
Phase 2
Section 13
(c) middle
Section 49
(b)
(a)
Section 15
(c) middle
Faraglione
Porto di Levante
Punte Nere
15
13
Punta Roia
Caruggi area
12
La Fossa di Vulcano
49
Rio Grande
Section 12
(c) middle
200 m
5
Palizzi area
(c) middle
Section 5

Fig. 8

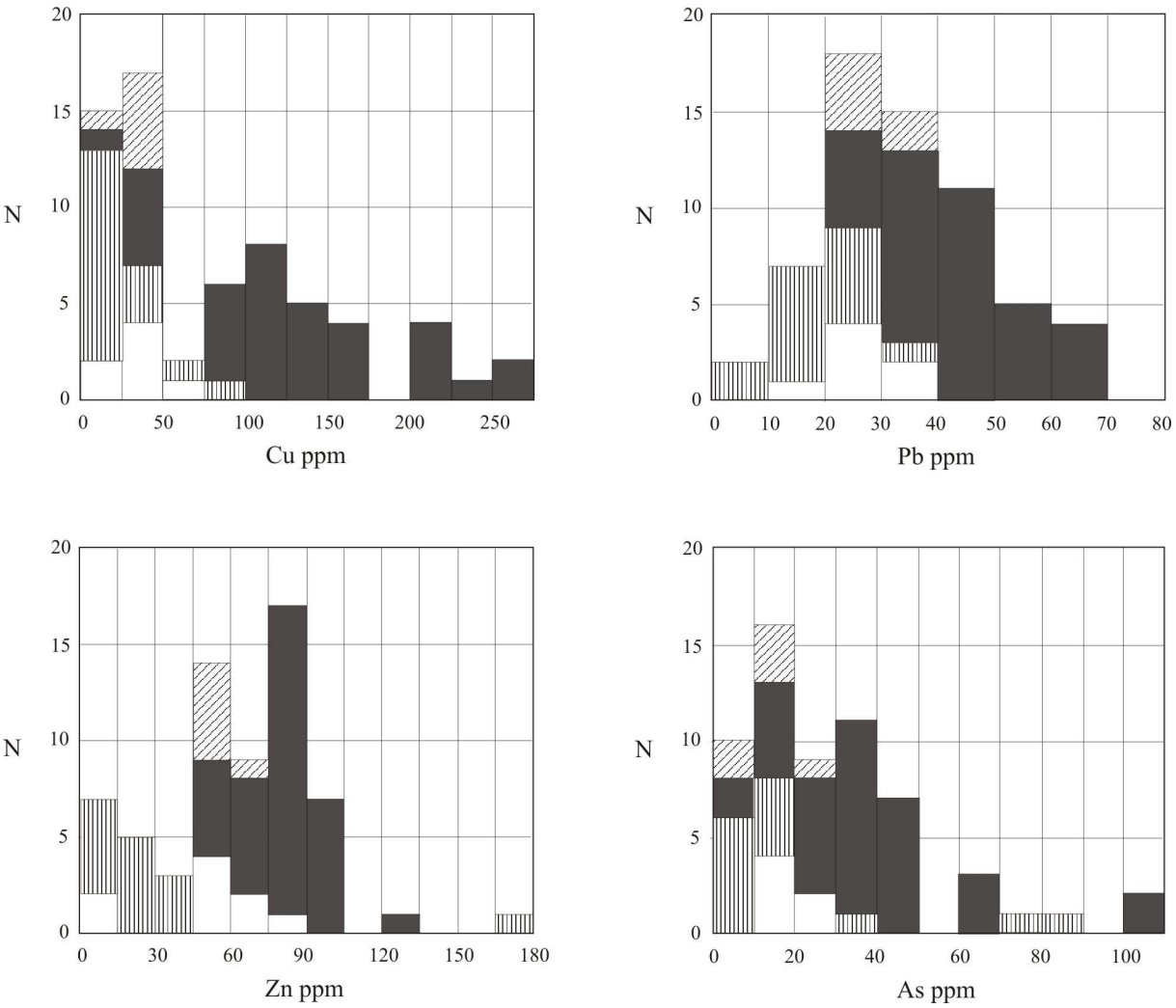
N
Cu ppm
Pb ppm
Zn ppm
As ppm

Fig.9

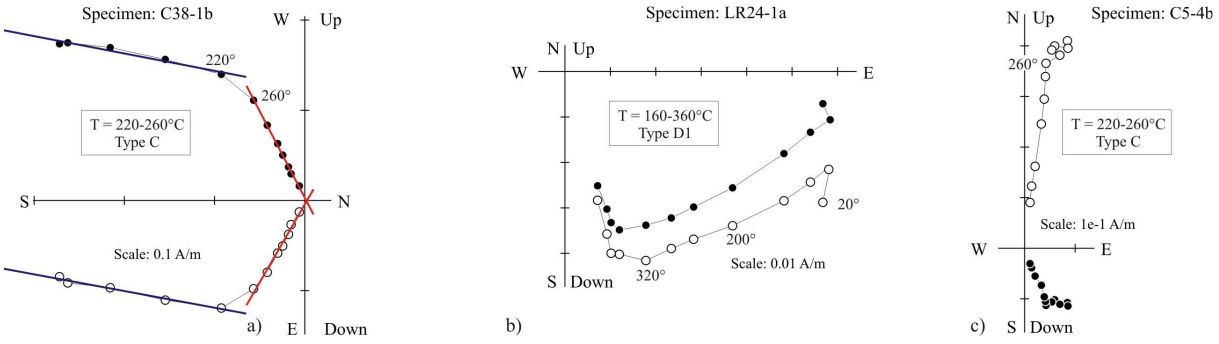
Specimen: C38-1b
T = 220-260°C
Type C
Scale: 0.1 A/m
a)
Specimen: LR24-1a
T = 160-360°C
Type D1
Scale: 0.01 A/m
b)
Specimen: C5-4b
T = 220-260°C
Type C
Scale: 1e-1 A/m
c)

Fig.10

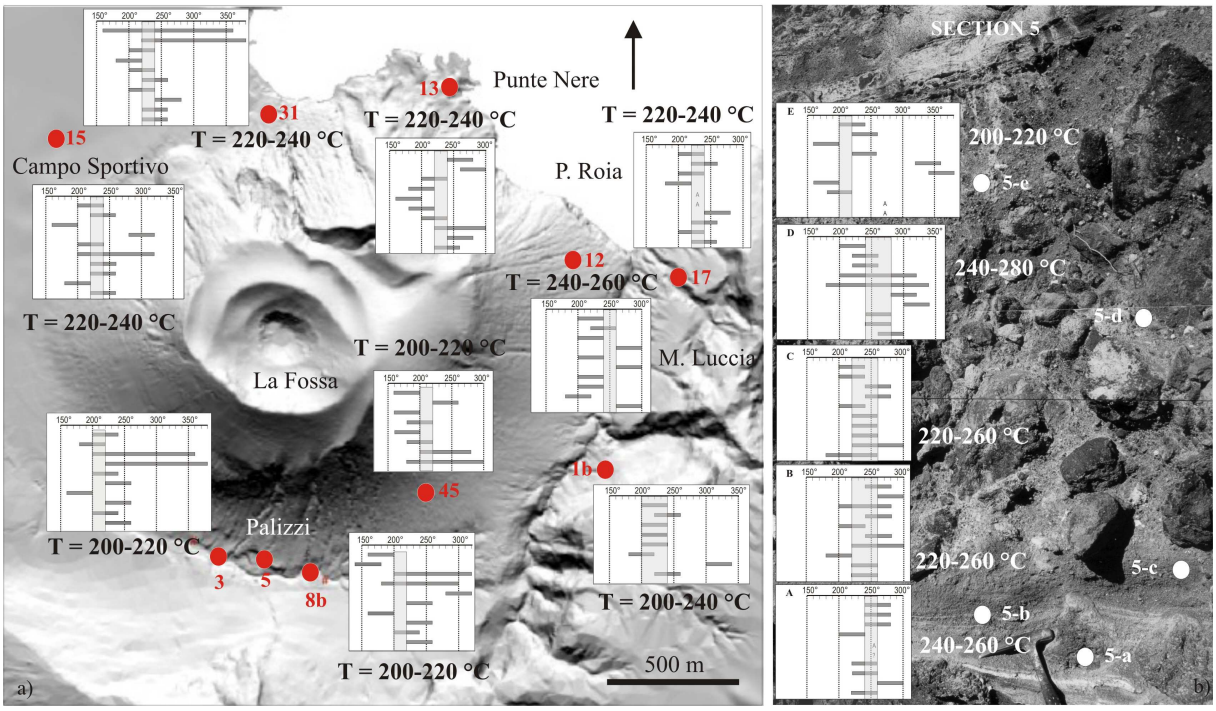
Punte Nere
13
T = 220-240 °C
T = 220-240 °C
31
T = 220-240 °C
15
Campo Sportivo
P. Roia
T = 220-240 °C
12
T = 240-260 °C
17
T = 220-240 °C
T = 200-220 °C
La Fossa
M. Luccia
45
1b
T = 200-220 °C
Palizzi
3
5
8b
T = 200-240 °C
T = 200-220 °C
500 m
a)
SECTION 5
200-220 °C
5-e
240-280 °C
5-d
220-260 °C
220-260 °C
5-c
5-b
240-260 °C
5-a
b)

Fig. 11

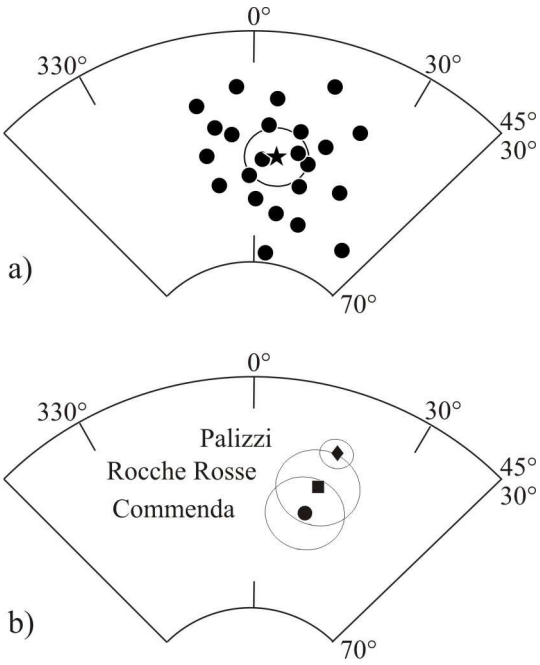
0°
330°
30°
45°
30°
a)
70°
0°
330°
30°
Palizzi
Rocche Rosse
Commenda
45°
30°
b)
70°

Fig. 12

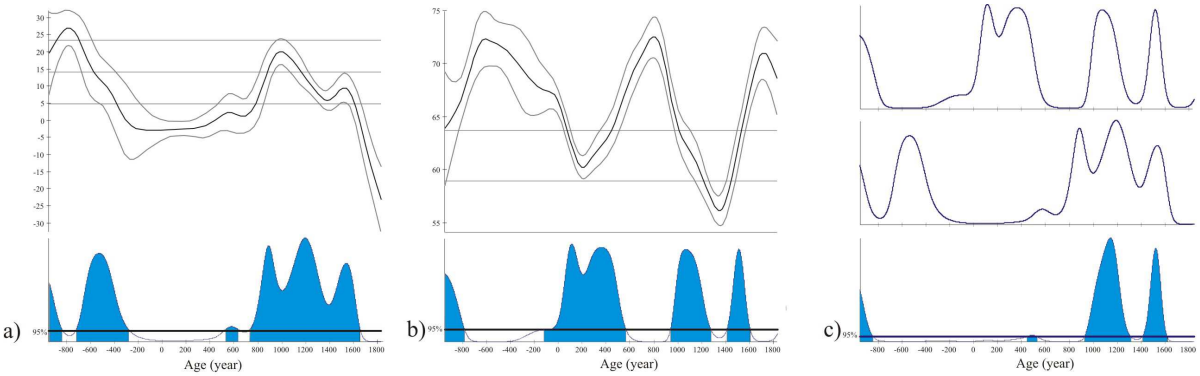

Fig. 13

	lapilli and bombs, bulk rock analysis			lapilli and bombs, glass analysis						coarse ash, glass analysis	
	trachyte	*rhyolite*									
		mean [5]	*SD*	*mean [8]*	*SD*	*mean [10]*	*SD*	*mean [3]*	*SD*	*mean [3]*	*SD*
SiO_2 (wt%)	64.47	68.66	1.04	72.55	1.40	72.58	0.73	62.19	0.64	68.38	0.31
TiO_2	0.38	0.27	0.03	0.11	0.02	0.14	0.04	0.44	0.02	0.21	0.09
Al_2O_3	15.75	14.61	0.58	14.18	1.10	13.94	0.34	17.87	0.17	15.74	0.37
Fe_2O_3tot	4.89	3.79	0.23	1.91	0.41	1.38	0.40	4.82	0.23	3.02	0.31
MnO	0.10	0.09	0.01	b.d.l.		b.d.l.		b.d.l.		b.d.l.	
MgO	1.49	0.97	0.18	0.25	0.04	0.23	0.04	1.39	0.00	0.81	0.03
CaO	3.20	2.17	0.17	1.34	1.87	0.52	0.31	2.19	0.04	1.23	0.06
Na_2O	4.27	4.15	0.11	3.41	1.64	4.39	0.62	3.01	0.43	3.76	0.13
K_2O	5.25	5.17	0.33	6.44	0.42	6.56	0.81	7.65	0.22	6.33	0.34
P_2O_5	0.20	0.13	0.02	b.d.l.		b.d.l.		b.d.l.		b.d.l.	
Cl	-	-	-	0.30	0.12	0.18	0.08	0.35	0.06	0.43	0.04
	100.00	100.00		100.50		99.92		99.91		99.91	

Table 1